

SEARCH FOR A SIGNATURE OF TWIST-REMOVAL IN THE MAGNETIC FIELD OF SUNSPOTS IN RELATION WITH MAJOR FLARES

OLGA BURTSEVA¹, SANJAY GOSAIN¹, AND ALEXEI A. PEVTSOV^{1,2}

¹National Solar Observatory, Boulder, CO 80303, USA

²ReSoLVE Centre of Excellence, Space Climate research unit, 90014 University of Oulu, Finland

ABSTRACT

We investigate the restructuring of the magnetic field in sunspots associated with two flares: the X6.5 flare on 6 December 2006 and the X2.2 flare on 15 February 2011. The observed changes were evaluated with respect to the so-called twist-removal model, in which helicity (twist) is removed from the corona as the result of an eruption. Since no vector magnetograms were available for the X6.5 flare, we applied the azimuthal symmetry approach to line-of-sight magnetograms to reconstruct the pseudo-vector magnetic field and investigate the changes in average twist and inclination of magnetic field in the sunspot around the time of the flare. For the X2.2 flare, results from the full vector magnetograms were compared with the pseudo-vector field data. For both flares, the data show changes consistent with the twist-removal scenario. We also evaluate the validity of the azimuthal symmetry approach on simple isolated round sunspots. In general, the derivations based on the azimuthal symmetry approach agree with true-vector field data though we find that even for symmetric sunspots the distribution of the magnetic field may deviate from an axially symmetric distribution.

Keywords: Sun: flares - Sun: magnetic fields - Sun: photosphere

1. INTRODUCTION

Flares are often seen as a tumultuous breakup of a previously stable configuration leading to the release of a significant amount of energy, material eruption, particle acceleration, and restructuring of the magnetic field. This magnetic restructuring may be a key for understanding the physics of processes taking place in the solar atmosphere in response to flares. [Hudson \(2000\)](#) suggested a coronal implosion scenario, when during a flare or CME eruption, the coronal field contracts toward lower atmospheric heights to reduce the magnetic energy stored prior to eruption, resulting in the field becoming more horizontal at the photospheric level. Since then several authors reported an increase of the horizontal field at the polarity inversion line (PIL) during flares (e.g., [Gosain & Venkatakrishnan 2010](#); [Wang & Liu 2010](#); [Petrie 2012](#)), rapid change in inclination angle (e.g., [Gosain & Venkatakrishnan 2010](#); [Gosain 2012](#); [Liu et al. 2012](#)), and other signatures of contraction of magnetic fields (e.g., [Li et al. 2009](#); [Wang et al. 2012](#)). These observed changes support the early interpretation of eruptions in the framework of the tether-cutting model (e.g., [Moore et al. 2001](#)).

Rapid, “permanent” (or long-lasting) changes associated with the impulsive phase of flares were also observed in longitudinal fields. For example, [Sudol & Harvey \(2005\)](#) found permanent post-flare changes in line-of-sight (LOS) magnetic fields measured with the Global Oscillation Network Group (GONG) instruments. Most of the changes took place in sunspot penumbrae, and occurred in less than 10 minutes during the impulsive phase of the flare. They also noted that the changes in magnetic field could be associated with a rapid penumbral decay (when a portion of penumbra suddenly vanishes after the flare) reported by other observers (e.g., [Liu et al. 2005](#)). [Sudol & Harvey \(2005\)](#) and [Liu et al. \(2005\)](#) found roughly an equal number of cases of longitudinal flux increase and decrease as the result of a flare, which seems to be at odds with the coronal implosion scenario. If the magnetic field contracts back to lower atmospheric heights, the field should always become more horizontal. [Petrie & Sudol \(2010\)](#) further analyzed flare-related changes in GONG LOS magnetograms, and found that an increase/decrease in longitudinal fields does not correspond straightforwardly to a decrease/increase in field inclination relative to the local vertical direction. However, the distribution of longitudinal field increases and decreases at different parts of active regions was found

to be consistent with Hudson’s loop-collapse scenario. It may be noted that flare-related changes identified only in vertical/LOS or horizontal components of the magnetic field may be a subject to an ambiguity, since either a change in the field strength or inclination angle or both could be responsible for the changes in vertical and/or horizontal components.

The implosion scenario gained significant support in published literature. However, it does not explain all (global) changes in magnetic field observed during the flares and hence, there is a need to explore other scenarios. For example, [Petrie \(2012\)](#) and [Kazachenko et al. \(2015\)](#) studied changes in the vector magnetic field in NOAA active region 11158 during the X2.2 flare, and while they reported the increase in the horizontal field at the PIL, which is consistent with the loops’ contraction, they also found an abrupt decrease in magnetic-field twist. To explain the latter, one might consider an alternative scenario based on magnetic helicity transport through the solar atmosphere. Many flare models employ the concept of twisted magnetic flux structures. The basic assumption is that the pre-flare configuration has excessive twist and (some of) this twist is removed from the corona as the result of eruption. The evolution of twist in the flux tube after the eruption could be understood in the framework of the [Longcope & Welsch \(2000\)](#) model of the emergence of a twisted flux tube through the photosphere into the corona. [Longcope & Welsch \(2000\)](#) concluded that the expansion of the coronal portion of the tube redistributes the twist between subphotospheric and coronal parts, which in its turn creates an imbalance of torque at the photosphere-corona interface. To maintain the balance of torque, the coronal portion of the flux tube should have its twist reduced. The evolution of magnetic twist in emerging active regions observed by [Pevtsov et al. \(2003\)](#) was found to be in agreement with [Longcope & Welsch \(2000\)](#) predictions. [Pevtsov et al. \(2003\)](#) (see also [Pevtsov 2008](#)) made a conjecture that the subphotospheric portion of flux “tubes” forming sunspots and active regions may serve as a reservoir of twist (helicity) for repeated flare and CME eruptions. When twist is removed from coronal fields (for example, via flares or CMEs), subphotospheric fields will re-supply twist and establish a new equilibrium in torque in about one day. This transport of twist may exhibit itself as rotational motion of the sunspot relative to its central point. The time for establishing a new equilibrium is largely determined by the Alfvén speed for the subphotospheric portion of the flux tube. [Pevtsov \(2012\)](#) described several cases of flares associated with rotating sunspots. The speed of sunspot rotation was slowing down prior to flares, but after the flares, it was increasing again. [Pevtsov \(2012\)](#) interpreted this as an indication of twist (helicity) transport through the solar atmosphere, when the sunspot rotation was a response to removal of helicity from the coronal portion of the flux system. The importance of twist in flares is also supported by recent observations: [Ravindra et al. \(2011\)](#), and [Inoue et al. \(2011\)](#) who conducted limited case studies and found that magnetic twist increases about one day or longer before flare onset and quickly decreases after the flare.

Unlike the tether-cutting (TC) model, a twist-removal (TR) model allows for a rapid restoration of conditions leading to the flare and/or CME, and it can explain a sequential, multi-day flaring “spree” of an active region. Several other phenomena such as rotating sunspots ([Brown et al. 2003](#)) and higher flare productivity for active regions with a strong pattern of kinetic helicity below them ([Reinard et al. 2010](#)) seem to support the TR-model. Thus, for example, [Pevtsov’s \(2012\)](#) study of rotating sunspots suggests that the amplitude of rotation increases after a major burst of flares in an active region, which suggests that rotation could be a reaction to the removal of twist from active region magnetic fields. Sudden removal of twist from the magnetic field will make the field more vertical, contrary to the coronal impulsion scenario.

Both TC and TR scenarios may take place on the Sun. Sudden removal of some twist, by itself, would decrease the azimuthal component of the field in a cylindrical flux tube, making the field more vertical. Removal of twist, however, also decreases the free energy of the field, which should deflate the field as noted by [Hudson \(2000\)](#). Deflating the field could amplify any remaining tilt, perhaps restoring part of the field’s azimuthal component.

In this work, we investigate the magnetic restructuring associated with two flares, the X6.5 flare on 6 December 2006 and the X2.2 flare on 15 February 2011. We evaluate the observed changes in a search for change in the twist of the magnetic field, which could support the twist-removal model. Since true-vector data are not available, in our study of the X6.5 flare, we use only LOS magnetograms. For this event, we employ the approach of azimuthal symmetry to reconstruct three components of (pseudo-)vector of magnetic field, and we use this data to investigate the changes in twist and inclination of (pseudo-)vector magnetic fields as the results of flares. Although the application of this method is limited to flares associated with relatively symmetric sunspots, it can be used for events not observed by vector magnetographs, such as, for example, the Helioseismic and Magnetic Imager (HMI) on board the Solar Dynamics Observatory (SDO) ([Pesnell et al. 2012](#)) or Hinode/SOT (Solar Optical Telescope; [Kosugi et al. \(2007\)](#)). For the X2.2 flare, we verify the reconstruction results from the azimuthal symmetry approach with the derivations based on full vector magnetograms from HMI. We also evaluate the validity of the azimuthal approach on simple, round, isolated sunspots. The rest of the article is organized as follows. In Section 2, we formulate the principles

of azimuthal (cylindrical) symmetry for reconstructing three components of the pseudo-vector field from LOS data. Section 3 discusses changes in orientation of the pseudo-vector field in relation with the X6.5 flare on 6 December 2006. Section 4 describes and compares the changes in magnetic field derived both from true and pseudo-vector data. Section 5 analyzes the applicability of azimuthal symmetry to magnetically isolated round sunspots, and Section 6 presents the critical discussion of the main findings of this work.

2. DERIVATION OF THE PSEUDO-VECTOR MAGNETIC FIELD

Let us describe a vector magnetic field in a cylindrical coordinate system with the origin at the center of the sunspot, azimuth angle, φ , and distance from the origin, r , by $\{B_z, B_R, B_\varphi\}$, the vertical (up-down), radial (inward-outward), and tangential (clock-counter clockwise) components, respectively. Reference (zero) azimuth is toward solar disk center and azimuth increases in the clockwise direction. Then, the line-of-sight component, B_{LOS} , can be written as (see [Pevtsov & Peregud 1990](#), for more details):

$$B_{LOS}(r, \varphi) = \cos \theta B_z(r, \varphi) + \sin \theta \cos \varphi B_R(r, \varphi) - \sin \theta \sin \varphi B_\varphi(r, \varphi) \quad (1)$$

where θ is the heliocentric distance of the sunspot. Assuming cylindrical symmetry, i.e., B_z , B_R , and B_φ are only functions of r , but not φ , the three field components can be computed as

$$\begin{aligned} B_z(r) &= \frac{1}{2\pi \cos \theta} \int_0^{2\pi} B_{los}(r, \varphi) d\varphi \\ B_R(r) &= \frac{1}{\pi \sin \theta} \int_0^{2\pi} B_{los}(r, \varphi) \cos \varphi d\varphi \\ B_\varphi(r) &= \frac{-1}{\pi \sin \theta} \int_0^{2\pi} B_{los}(r, \varphi) \sin \varphi d\varphi \end{aligned} \quad (2)$$

The cartoon in Figure 1 represents the sign convention for the pseudo-vector field components: negative B_z and B_R are in the downward and “into the sunspot” direction, respectively, and negative B_φ corresponds to the clockwise direction. Figure 1 also shows an example of distribution of the horizontal components of the magnetic field in round sunspot NOAA 11084 with the same sign (as in the cartoon) of B_z , B_R , and B_φ .

The pseudo-vector calculations could be used to investigate twist reduction and loop collapse via changes in the B_z , B_R , and B_φ components, and field component $B_h = \sqrt{B_R^2 + B_\varphi^2}$. Twist reduction would imply a decrease in B_φ and possibly an increase in B_z . Loop collapse would give an increase of B_h (and possibly a decrease of B_z). The pseudo-vectors could help to discriminate between loop collapse and twist reduction with a large number of pre-SDO (and, in particular, GONG) observations, which would be important to this cycle with such a relatively small number of flares. Two of such major flares are discussed in more detail in the following sections.

3. FLARE-RELATED MAGNETIC FIELD CHANGES: X6.5 FLARE ON 6 DECEMBER 2006

The X6.5 flare on 6 December 2006, which occurred in NOAA active region 10930, was a white-light flare, associated with a Moreton wave and coronal mass ejection ([Balasubramaniam et al. 2010](#)). In the upper panel in Figure 2, the image from the Optical Solar Patrol Network (OSPAN, later known as the Improved Solar Observing Optical Network, ISOON ([Neidig et al. 1998](#))) shows a white light flare at about 18:45 UT and a stepwise reduction in penumbral area (courtesy of [Petrie et al. \(2012\)](#), see also [Balasubramaniam & Henry \(2016\)](#)). The flare was observed by GONG instruments. GONG full-disk magnetograms are obtained with 1-minute cadence, 2.5-arcsec pixel size, and 3 G per pixel noise level. Previous studies reported significant stepwise changes in the GONG LOS magnetic field associated with the flare ([Petrie & Sudol 2010](#); [Burtseva & Petrie 2013](#)). Analysis of the direction of the Lorentz force changes suggested the contraction of the field lines toward the neutral line resulting in a more horizontal magnetic field at the neutral line region ([Petrie & Sudol 2010](#)). [Burtseva & Petrie \(2013\)](#) found contraction of the field toward the neutral line in the form of flux cancellation events during the X6.5 flare, but no correlation between the flux cancellation and abrupt stepwise field changes associated with coronal field implosion. Using Hinode G-band white light and Ca II H – line broadband filtergrams, [Deng et al. \(2011\)](#) presented the rapid stepwise decay of the outer sunspot penumbra and enhanced, sheared Evershed flow near the flared neutral line, indicating weakening of horizontal field in the outer region and showing a more horizontal sheared magnetic field near the flared neutral line.

True-vector magnetic field observations at the time of this flare are not available, and thus, we employ the cylindrical symmetry approach to reconstruct the vertical, radial, and tangential components $\{B_z, B_R, B_\varphi\}$ of the vector magnetic

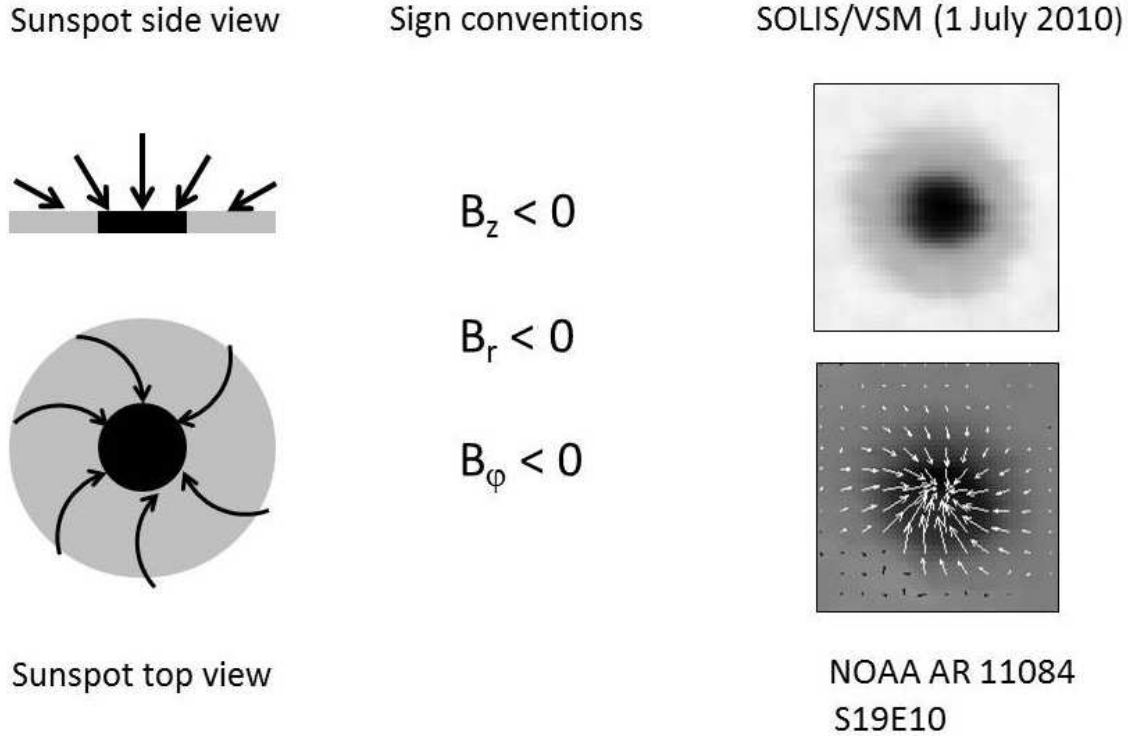


Figure 1. Cartoon explaining the sign convention for pseudo-vector field components. SOLIS/VSM continuum intensity at the top right and true-vector field observations at the bottom right with the vertical field component, B_z , as the background, with the horizontal components indicated by arrows. Dark halftones correspond to the negative polarity field, and the length of the arrows is proportional to horizontal field strength.

field following the approach presented in Section 2. Time evolutions of B_z (vertical) and B_ϕ (azimuthal) are shown in two lower panels in Figure 2. At the time of the flare, there is a clear indication of increase in the amplitude of the vertical field and the decrease in the amplitude of the azimuthal component. The radial B_R component (not shown) did not change significantly as the result of this flare. We interpret these changes as an indication that after the flare the magnetic field in penumbra became less twisted and more vertical, which is in general agreement with the expectations of the twist-removal model.

4. FLARE-RELATED MAGNETIC FIELD CHANGES: X2.2 FLARE ON 15 FEBRUARY 2011

An X-ray X2.2 flare occurred on 15 February 2011 in NOAA active region (AR) 11158. For this flaring region, both LOS and vector magnetograms were taken by SDO/HMI, and we use these observations to compare the changes in magnetic field twist derived from LOS data with those of true-vector field observations. HMI 12-minute LOS and vector magnetograms in the form of Active Region Patches (HARPs), maps of vertical and two horizontal field components $\{B_r, B_\theta, B_\phi\}$ with pixel size 0.03 degrees in heliographic coordinates derived by cylindrical equal-area (CEA) projection (see Hoeksema et al. 2014), have been used for this flare analysis. Here, B_θ and B_ϕ are the field components in the meridional and zonal direction, respectively.

We transform the transverse true-vector field $\{B_\theta, B_\phi\}$ to the radial and azimuthal field components $\{B'_R, B'_\phi\}$ in cylindrical geometry as (see Venkatakrisshnan & Tiwari 2009):

$$B'_R = \frac{1}{r}(xB_\phi + yB'_\theta)$$

$$B'_\phi = \frac{1}{r}(-yB_\phi + xB'_\theta)$$

where x and y equal zero in the sunspot center, and $B'_\theta = -B_\theta$ (see Sun 2013, for details). The vertical field component $B_z = B_r$. Here, B_r refers to Venkatakrisshnan & Tiwari (2009) notation for vertical component, which is

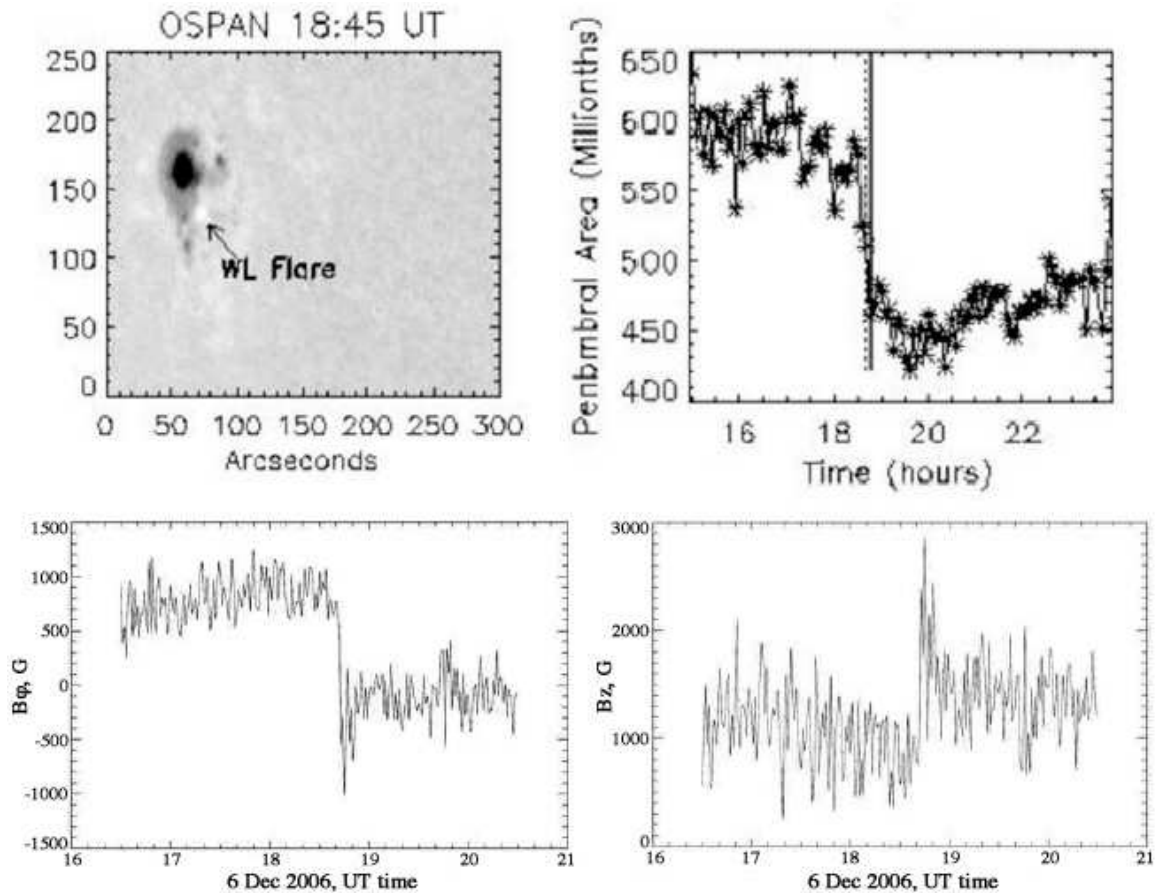


Figure 2. White light image from OSPAN (upper-left) with a white light flare at about 18:45 UT and a corresponding step-wise reduction in area of penumbra (upper-right). Two lower panels show time evolution of vertical (B_z , lower-right) and azimuthal (B_ϕ , lower-left) components of the pseudo-vector reconstructed under the assumption of cylindrical symmetry. Vertical lines in the upper-right panel mark start and peak times of this flare in white light intensity.

B_z in our notation.

We obtain azimuthal averages of the true-vector $\{B_z^v, B_R^v, B_\phi^v\}$ and pseudo-vector $\{B_z, B_R, B_\phi\}$ magnetic field components using Eq. 2 as a function of distance from sunspot center, r .

The active region NOAA 11158 had a complex structure with four sunspots. Two of them were involved in the flare. This part of the active region with two sunspots is shown in Figure 3. The shapes of the sunspots can be partly considered as round with complex inclusions in their penumbras. Based on the distribution of horizontal fields (Figure 3 right), the sunspot of positive polarity (white halftones) appears reasonably symmetric, and thus, is considered to be suitable for the application of the cylindrical symmetry approach. The sunspot of negative polarity (left side of panel) has an elongated shape, and its umbra is divided by a light bridge. Still, based on the orientation of the horizontal field, the portion of the sunspot to the left of the light bridge appears quite symmetric, and thus, the assumption of cylindrical symmetry was applied to this sunspot too.

Profiles of the pseudo-vector $\{B_z, B_R, B_\phi\}$ along with azimuthally averaged true-vector $\{B_z^v, B_R^v, B_\phi^v\}$ field components in the negative polarity sunspot at pre-flare and post-flare times are shown in Figure 4. Average profiles of the vertical B_z component (Figure 4, middle) derived from Eq. 2 (pseudo-vector, solid lines) and by azimuthal averaging of true vector (dashed lines) show similar changes with distance from the center of the sunspot ($r/R = 0$). Still, the B_z from the pseudo-vector shows much weaker field strengths in umbral area (1400-1600 Gauss vs. 2000 Gauss), and they decrease less steeply with the radial distance from the sunspot center. Both approaches give similar average field strengths at the outer boundary of the sunspot (about 600 Gauss). The radial B_r and azimuthal (tangential) B_ϕ components show more differences between pseudo- and true-vector data. The true-vector component B_R gradually increases from umbra to the umbra-penumbra boundary, and it decreases outward to the outer penumbra boundary ($r/R = 1$). The pseudo-vector shows a slight decrease in the radial (with respect to radial direction away from sunspot

center) component of the field, and it significantly increases at approximately middle of the penumbra. In the sunspot umbra, the azimuthal (tangential) component derived from assumption of cylindrical symmetry has a similar amplitude to the azimuthally averaged B_φ from the true vector, but it increases much more steeply toward the outer penumbral sunspot boundary. Comparing the amplitudes of the vertical and horizontal fields, on average, the true-vector field yields a less inclined vector (about 30-35 degrees relative to the vertical direction at the umbra-penumbra boundary and 40-45 degrees in the middle of the penumbra) as compared with the pseudo-vector (50-55 degrees in the middle of the penumbra). Thus, despite the overall agreement in sign of the three components of the vector field and similar behavior (decrease-increase) in the radial direction from the sunspot center to its outer boundary, the profiles of the three components look quite different between the two methods in their amplitudes and the steepness of center-to-boundary variation. Similar differences could be noted in pre-/post-flare changes. The absolute and fractional (relative to true-vector) discrepancies in total flux of the sunspot between the pseudo- and true-vector method are about 2.66×10^{17} Mx and 0.15, respectively.

The vertical component (Figure 5, middle panel) of the true-vector field (dashed lines) shows some evidence of a slight decrease in the sunspot umbra as the result of the flare. The pseudo-vector data show a similar decrease, but, unlike the true-vector, such a decrease is observed in both umbra and penumbra. The largest difference between the two approaches can be seen in the B_R and B_φ components (left and right panels). The radial component in the pseudo-vector (left panel) exhibits strong increase after the flare, while the azimuthally averaged true vector does not show any significant change in B_R .

The azimuthal component of the true-vector field decreases in the sunspot umbra and increases in the outer penumbra as a result of the flare. This is consistent with the field becoming more horizontal in the penumbra. The azimuthal (tangential) component of the pseudo-vector field decreases in the sunspot umbra in agreement with the true-vector measurements. B_φ from the pseudo-vector increases in the outer penumbra similarly to the true vector, although the latter does not show a strong stepwise change as the former does. Overall, the changes in the three components of the vector field derived by two methods could be interpreted as an indication of reduction in twist in umbral fields although the evolution of penumbral fields is less clear in that respect.

No clear change in global properties of the field of the positive polarity sunspot in relation to the flare was found in either the pseudo-vector or the true-vector magnetic fields. Absence of the field changes in both true- and pseudo-vector field components suggests that flare-related changes could be local in their nature, and when averaged over the entire sunspot, these changes may not always be obvious.

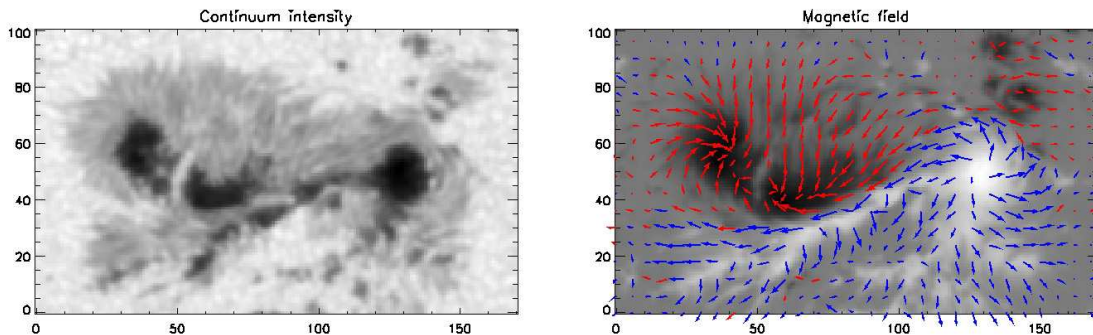


Figure 3. Continuum intensity (left) and vertical magnetic field in the active region NOAA 11158 with the horizontal field shown with arrows (right).

5. DISTRIBUTION OF MAGNETIC FIELD IN ISOLATED ROUND SUNSPOTS

Examples of flare-related changes in magnetic fields shown in Sections 3 and 4 indicate that, at least in some instances, the approach of computing the pseudo-vector field could yield useful information about the evolution of average twist in flaring regions, but the applicability of the method needs to be carefully evaluated. The discrepancies

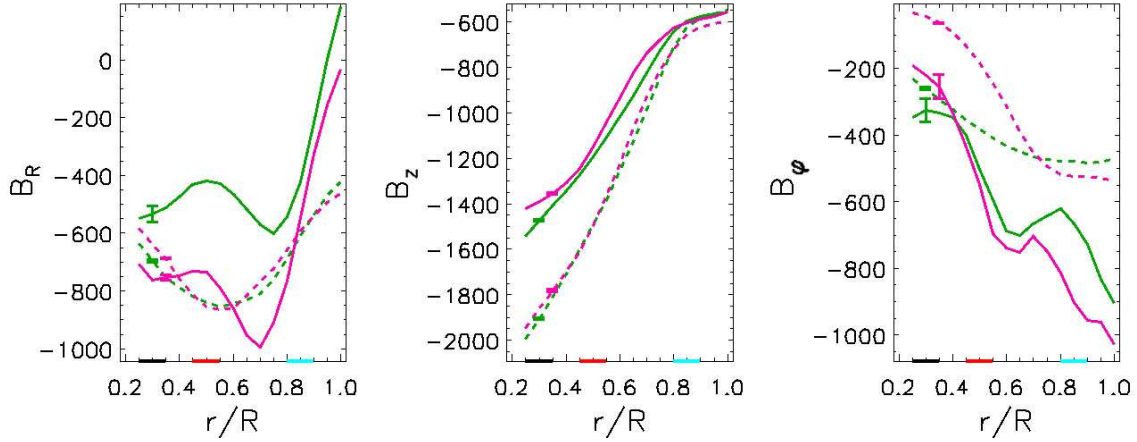


Figure 4. Pseudo-vector $\{B_z, B_R, B_\phi\}$ (solid line) and true-vector $\{B_z^y, B_R^y, B_\phi^y\}$ (dashed line) magnetic field components as a function of distance from the sunspot center in fractions of its radius, obtained for the negative polarity sunspot located at the flare site in the active region NOAA11158 on February 15, 2011 right before (green) and after (magenta) the flare. Error bars represent typical uncertainties of the measurements. Black, red, and cyan dashes along x -axes indicate umbra, umbra-penumbra boundary and penumbra regions, respectively, for temporal profiles in Figure 5.

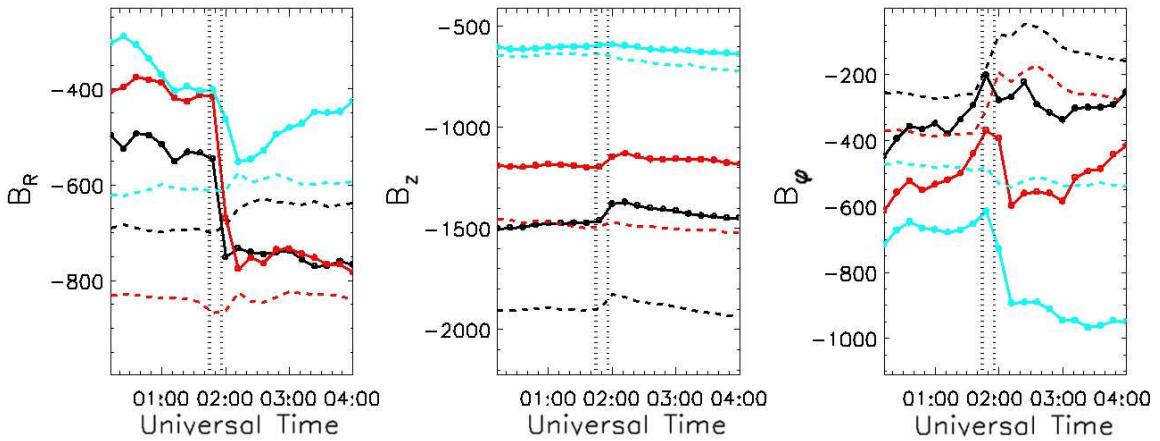


Figure 5. Temporal profiles of the three vector-field components in the NOAA active region 11158 on Feb 15, 2011 around time of the X2.2 flare. The results shown for the negative polarity sunspot located at the flare site. Solid curves correspond to the pseudo-vector and dashed curves obtained from true-vector observations in umbra (black), at the umbra-penumbra boundary (red), and in penumbra (cyan). Vertical dotted lines indicate GOES flare start, peak, and end times.

between the true- and pseudo-vector magnetic field in the flared active regions might arise due to the facts that the sunspots analyzed are not isolated, and they have asymmetries in their penumbras. For further validation of the cylindrical symmetry technique, we have selected 16 nearly round, isolated sunspots, listed in Table 1 (the X6.5 and X2.2 flare events are included in the Table as well). Fourteen of these sunspots were analyzed using magnetograms taken for about one-hour time spans, usually around the time when the sunspot was close to the solar central meridian. Two sunspots, a simple, round, uniformly twisted sunspot in active region NOAA 11084 and another round sunspot in NOAA active region 11899, were studied over the period of a few days as they crossed the solar disk within $\sim 45^\circ$ heliographic longitude from the solar disk center. The Pearson linear correlation coefficients for the azimuthal component of the pseudo- and true-vector magnetic fields for the 16 sunspots and their P -values, the probability that the observed correlation occurs by chance, computed using the t-test, are also shown in Table 1. Pseudo-vector $\{B_z, B_R, B_\phi\}$ along with azimuthally averaged true-vector $\{B_z^y, B_R^y, B_\phi^y\}$ field components for the NOAA 11084 on July 1, 2010 and NOAA11899 on November 20, 2013 are shown in Figure 6.

B_R and B_z components of pseudo-vector and azimuthally averaged true-vector field profiles seem to be in a good agreement with each other. In most of the sunspot ($R < 0.8$) from NOAA 11084, the amplitude of the tangential

Table 1. List of analyzed sunspots. Last column shows Pearson correlation coefficients (the P -values given in parentheses) for the azimuthal field component of the pseudo- and true-vector magnetic fields in the sixteen nearly round, isolated sunspots.

Date	Location	NOAA Number	Flare Event	Correlation Coefficient B_φ vs. B_φ^v
2006 Dec 6	S05E64	10930	X6.5	
2010 Jun 28 - - Jul 6	S19E45 S19W50	11084	B1.0 (Jul 1)	-0.92 (3.55×10^{-15})
2010 Aug 4	N12W07	11092		0.61 (5.24×10^{-5})
2010 Aug 31	N12W05	11101		-0.06 (0.76)
2010 Oct 21	S29W01	11115		0.81 (6.90×10^{-9})
2010 Dec 10	N31W21	11133		0.48 (2.29×10^{-3})
2011 Jan 21	N24E05	11147		0.62 (1.01×10^{-3})
2011 Feb 15	S20W10	11158	X2.2	
2011 Apr 19	N17E01	11193		0.79 (4.81×10^{-8})
2011 Apr 24	S16W01	11195		-0.36 (5.34×10^{-2})
2011 Oct 10	N23W01	11312		-0.22 (0.24)
2011 Nov 10	S08W01	11340		0.09 (0.69)
2012 Mar 29	S23E07	11445		0.88 (1.48×10^{-12})
2012 Sep 30	S10W01	11579		0.91 (8.66×10^{-15})
2012 Oct 18	N07E05	11591		-0.23 (0.24)
2013 Nov 15 - - Nov 20	N07E37 N05W29	11899		0.73 (4.64×10^{-11})
2014 Feb 13	S15E11	11976		0.15 (0.41)
2016 Apr 26	S02W03	12533		0.57 (2.85×10^{-3})

(azimuthal) component of the magnetic field derived under the assumption of cylindrical symmetry (B_φ) is larger than the azimuthally averaged azimuthal component of the true-vector field (B_φ^v). The true-azimuthal field B_φ^v is close to zero near the sunspot center and then starts rising slowly, which is opposite to the trend of the pseudo-azimuthal field B_φ in the sunspot umbra and inner penumbra, resulting in a negative correlation between them (see Table 1). There was a small (B1.0) X-ray flare in NOAA11084 on July 1 at 20:54 UT. Changes in inclination angle in NOAA11084 as it passed the solar disk, shown in Figure 6, seem to suggest that the magnetic field in the sunspot penumbra became slightly more vertical after the flare (inclination angle decreases), and then becomes more horizontal (inclination angle increases) again during the time span of one (one and half) day, which is in qualitative agreement with the twist-removal model, when helicity (twist) removed from a flaring/CME source active region can be replenished from below the photosphere within one or two days (e.g., [Pevtsov 2008](#)).

For active region NOAA 11899 (Figure 6, panels (C) and (F)) the sign and the general trend of azimuthal B_φ components of both the true- and pseudo-vector fields are in good qualitative agreement with each other. B_R derived from cylindrical symmetry shows a more complicated variations with radial distance from sunspot center, as compared with B_R^v (Figure 6, panels (C) and (F)).

Analysis of other 14 round sunspots indicates that the cylindrical symmetry approach does, in general, provide a correct sign of the pseudo-vector field components, but the trend of the pseudo-vector components as a function of radial direction from sunspot center can be different from that derived from the true-vector field. Also, the amplitude of the pseudo-vector field variations along the sunspot radius is often much larger than the variations in the true-vector field. Scatter plots of the true- and pseudo-vector field values computed along the radial direction in the 16 isolated sunspots in Figure 7 summarize the results. The Pearson linear correlation coefficients for the B_R , B_z , and B_φ components of the pseudo- and true-vector magnetic fields are 0.90, 0.99, and 0.31 and their P -values are 0.0, 0.0, and 1.8×10^{-12} , respectively, revealing a strong correlation for the B_R and B_z components and weak correlation for the B_φ component, in general. The B_φ component of the pseudo- and true-vector magnetic fields in only half of the 16 sunspots reveals a statistically significant positive moderate or strong correlation (see Table 1).

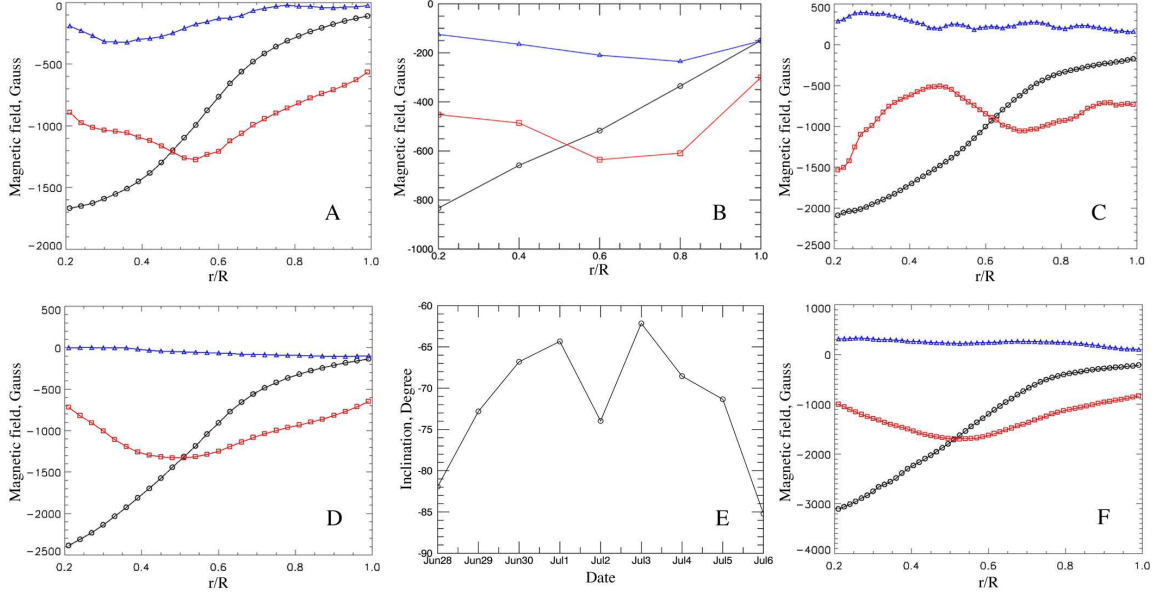


Figure 6. Three components of magnetic field as a function of radial distance from sunspot center ($R=0$) to sunspot outer penumbra boundary ($R=1$). Pseudo-vector magnetic field components B_z (black circles), B_R (red squares), and B_ϕ (blue triangles) in cylindrical symmetry obtained from (A) HMI and (B) SOLIS/VSM photospheric longitudinal magnetic field in the NOAA11084 on July 1, 2010. (D) Azimuthally averaged magnetic field components as a function of distance from the sunspot center in fractions of its radius obtained from HMI vector data. (C) and (F) Pseudo-vector and true-vector magnetic field components, respectively, for the NOAA11899 on Nov 20, 2013. (E) Inclination angle in NOAA11084 computed in the penumbra at $R=0.75$ of the sunspot's radius as the active region crosses the solar disk.

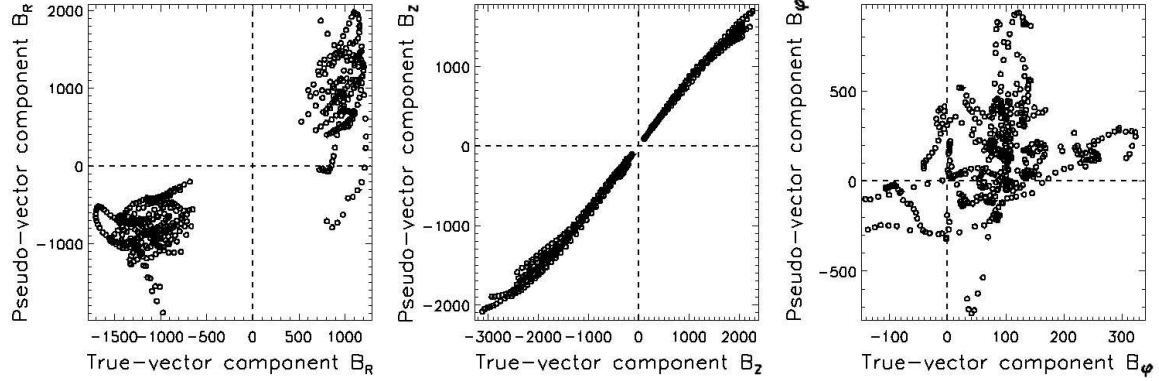


Figure 7. Scatter plot of the pseudo-vector as a function of the true-vector magnetic field values, computed along the radial direction in the 16 round, isolated sunspots listed in Table 1.

6. DISCUSSION

In this work, we analyzed magnetic field changes associated with two flares, the X6.5 flare on 6 December 2006 and X2.2 flare on 15 February 2011. In particular, we used the data to search for a signature of removal of twist as the result of flares. We applied the azimuthal symmetry approach to investigate the changes in twist and inclination of magnetic field in two sunspots that hosted major X-ray flares (X6.5 flare in AR NOAA 11084 and X2.2 flare in AR NOAA 11158). For the latter active region, we compared the results with the azimuthally averaged true-vector field. For both active regions, we found the changes in orientation of magnetic field consistent with the twist-removal scenario.

However, our study also raises some questions about the applicability of the cylindrical symmetry approach. While the pseudo-vector field revealed some of the abrupt changes in the magnetic field associated with X-class flares, the amplitude and/or the sign of these changes does not always clearly agree with changes derived from true-vector field

data. The shapes of the sunspots can only partly be considered as round. The cylindrical (azimuthal) symmetry approach could be more readily justified in isolated round sunspots, but even for such sunspots, the derived pseudo-vector components may disagree with azimuthally averaged true-vector field components. Absence of clear flare-related field changes in both true- and pseudo-vector field components for one of the sunspots suggests that flare-related changes could be local in their nature, and when averaged over the entire sunspot, these changes may become less apparent.

Finally, we have investigated how well the azimuthal (cylindrical) symmetry approach works for isolated round sunspots. We found that the results from this approach agree with true vector for selected sunspots, but even for symmetric sunspots the distribution of twist may be complex. Figure 8 (panel (D)) shows the distribution of the longitudinal (LOS) component of the magnetic field as a function of azimuthal angle at a fixed distance from the center of a sunspot. The variation of B_{LOS} with azimuth does change in a manner similar to the expected behavior (namely, as if at different azimuths, B_{LOS} represents the LOS projection of the same vector field). However, this variation does not agree exactly with changes one would derive using Eq. 1 under the assumption that B_z , B_r , and B_ϕ components of that vector are constant (solid line in Figure 8d). Figure 8 (panels (A)–(C)) shows the variation of each component of a true vector as a function of azimuth. The horizontal dashed line in each panel shows the mean value of this vector field component. It is clear that the azimuthal distribution of each of the three vector field components is not constant for a fixed radial distance from sunspot center. Out of three components, B_z (vertical) is approximately constant for range of azimuths between 0 and 260 degrees. Between 260 and 360 degrees, the mean value is quite different. Two other components show even less constancy with azimuthal angle inside the sunspot. For this sunspot, one could argue that B_r could still be considered “constant” within $\pm 15\text{--}20\%$. However, the azimuthal (B_ϕ) component even has opposite signs in different parts of the penumbra. These shortcomings of cylindrical (azimuthal) symmetry need to be taken into consideration in all future attempts to employ this type of model.

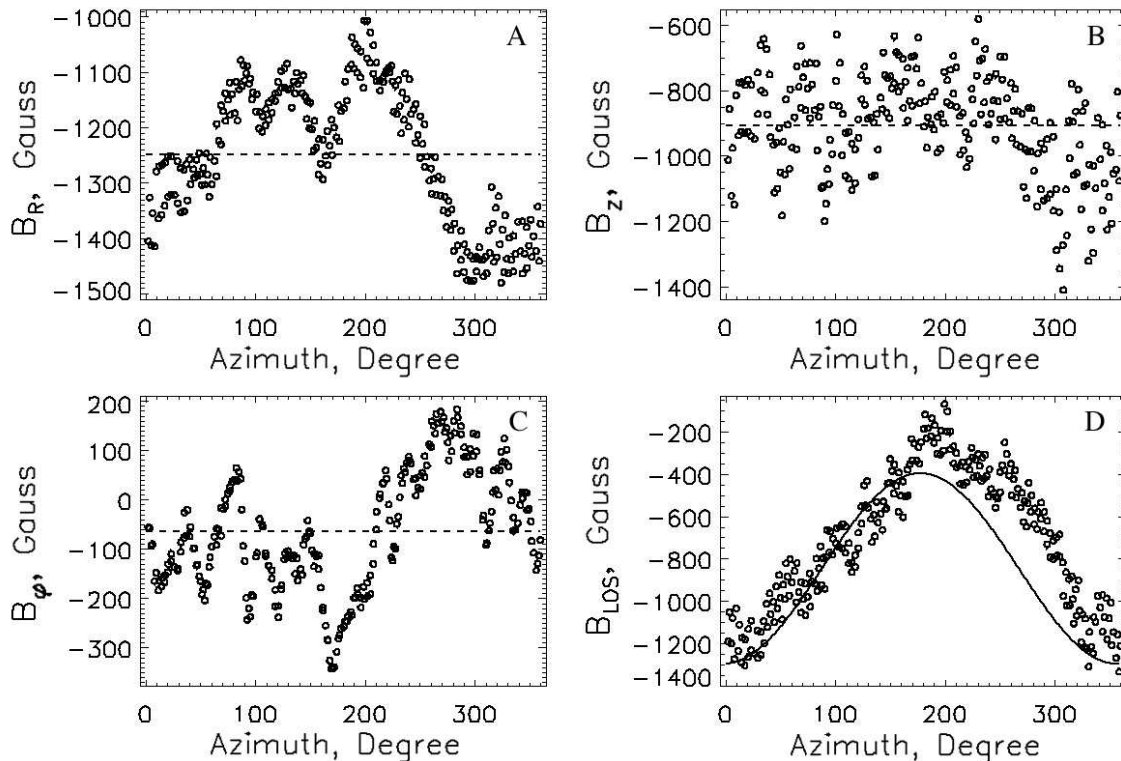


Figure 8. Variation of true-vector $\{B_z, B_R, B_\phi\}$ and LOS magnetic field components as a function of azimuth at $R=0.6$ of the sunspot’s radius for the sunspot in the active region NOAA11084 on July 1, 2010. Horizontal dashed lines in panels (A)–(C) indicate the mean value for each component. The solid curve in panel (D) shows the expected variation in B_{LOS} computed using mean B_z , B_R , and B_ϕ and Equation 1.

7. ACKNOWLEDGMENTS

The HMI data are provided by NASA/SDO and the HMI Science Team. GONG and SOLIS data obtained by the NSO Integrated Synoptic Program (NISP), managed by the National Solar Observatory, which is operated by the Association of Universities for Research in Astronomy (AURA), Inc. under a cooperative agreement with the National Science Foundation. Authors of this work are partially supported by NASA grant NNX14AE05G. A.A.P. acknowledges the financial support by the Academy of Finland to the ReSoLVE Centre of Excellence (project No. 272157).

REFERENCES

- Balasubramaniam, K. S., & Henry, T. W. 2016, *SoPh*, 291, 3123
 Balasubramaniam, K. S., Cliver, E. W., Pevtsov, A., et al. 2010, *ApJ*, 723, 587
 Brown, D. S., Nightingale, R. W., Alexander, D., et al. 2003, *SoPh*, 216, 79
 Burtseva, O., & Petrie, G. 2013, *SoPh*, 283, 429
 Deng, N., Liu, C., Prasad Choudhary, D., & Wang, H. 2011, *ApJL*, 733, L14
 Gosain, S. 2012, *ApJ*, 749, 85
 Gosain, S., & Venkatakrishnan, P. 2010, *ApJL*, 720, L137
 Hoeksema, J. T., Liu, Y., Hayashi, K., et al. 2014, *SoPh*, 289, 3483
 Hudson, H. S. 2000, *ApJL*, 531, L75
 Inoue, S., Kusano, K., Magara, T., Shiota, D., & Yamamoto, T. T. 2011, *ApJ*, 738, 161
 Kazachenko, M. D., Fisher, G. H., Welsch, B. T., Liu, Y., & Sun, X. 2015, *ApJ*, 811, 16
 Kosugi, T., Matsuzaki, K., Sakao, T., et al. 2007, *SoPh*, 243, 3
 Li, Y., Jing, J., Tan, C., & Wang, H. 2009, *Science in China: Physics, Mechanics and Astronomy*, 52, 1702
 Liu, C., Deng, N., Liu, Y., et al. 2005, *ApJ*, 622, 722
 Liu, C., Deng, N., Liu, R., et al. 2012, *ApJL*, 745, L4
 Longcope, D. W., & Welsch, B. T. 2000, *ApJ*, 545, 1089
 Moore, R. L., Sterling, A. C., Hudson, H. S., & Lemen, J. R. 2001, *ApJ*, 552, 833
 Neidig, D., Wiborg, P., Confer, M., et al. 1998, in *Astronomical Society of the Pacific Conference Series*, Vol. 140, *Synoptic Solar Physics*, ed. K. S. Balasubramaniam, J. Harvey, & D. Rabin, 519
 Pesnell, W. D., Thompson, B. J., & Chamberlin, P. C. 2012, *SoPh*, 275, 3
 Petrie, G., Balasubramaniam, K. S., Burtseva, O., & Pevtsov, A. A. 2012, in *American Astronomical Society Meeting Abstracts*, Vol. 220, *American Astronomical Society Meeting Abstracts #220*, 204.06
 Petrie, G. J. D. 2012, *ApJ*, 759, 50
 Petrie, G. J. D., & Sudol, J. J. 2010, *ApJ*, 724, 1218
 Pevtsov, A. A. 2008, *Journal of Astrophysics and Astronomy*, 29, 49
 —. 2012, *Astrophysics and Space Science Proceedings*, 30, 83
 Pevtsov, A. A., Maleev, V. M., & Longcope, D. W. 2003, *ApJ*, 593, 1217
 Pevtsov, A. A., & Peregud, N. L. 1990, *Washington DC American Geophysical Union Geophysical Monograph Series*, 58, 161
 Ravindra, B., Yoshimura, K., & Dasso, S. 2011, *ApJ*, 743, 33
 Reinard, A. A., Henthorn, J., Komm, R., & Hill, F. 2010, *ApJL*, 710, L121
 Sudol, J. J., & Harvey, J. W. 2005, *ApJ*, 635, 647
 Sun, X. 2013, *ArXiv e-prints*, arXiv:1309.2392
 Venkatakrishnan, P., & Tiwari, S. K. 2009, *ApJL*, 706, L114
 Wang, H., & Liu, C. 2010, *ApJL*, 716, L195
 Wang, S., Liu, C., Liu, R., et al. 2012, *ApJL*, 745, L17